Research Article

Received: 9 February 2026 Revised: 4 July 2026 Published online in Wiley Online Library:

(wileyonlinelibrary.com) DOI 10.1002/pi.70188

Iron(III) ion reinforced P(NiPAAm-*co*-AA) beads as tunable smart organogels

Johannes Gmeiner, Jonah Hasse and Gerrit A Luinstra*

Abstract

P(NiPAAm-*co*-AA) organogel beads were prepared by UV-induced droplet polymerization and mechanically reinforced through treatment with iron(III) chloride. Energy-dispersive X-ray spectroscopy mapping revealed a structure generation dependent on the amount of iron incorporation: beads with a low iron(III) loading have a core–shell architecture; high loadings result in a more homogeneous distribution of the ions over the particle volume. Fourier transform infrared analysis and proton release indicate coordination of iron(III) ions to formed carboxylic entities in the copolymer. A colorimetric thiocyanate assay allowed us to quantify the iron uptake, identifying a limit at a ratio of Fe^{3+} to COOH entities of approximately 1:3.8. The compressive Young's modulus of the 5 mm beads increased by a factor of 378 from 6.1 kPa in the parent gel to 2.3 MPa in the Fe^{3+}-saturated beads. The gels show a highly reversible shrinkage and swelling during solvent exchange between ethanol and ethyl acetate. The reinforced beads with a low and a high Fe^{3+} content conditioned in ethanol undergo a shrinkage of their volume after immersing in ethyl acetate of 38% and 25%, respectively; the time constants for shrinkage increase most significantly with the iron content; the rate of swelling is comparable. No iron(III) leaching was detected over multiple swelling–shrinkage cycles.

Supporting information may be found in the online version of this article.

Keywords: core–shell particle; ionic crosslinking; NiPAAm–acrylic acid copolymers; organogel beads; solvent-responsive smart materials

INTRODUCTION

Integrating stimulus-responsive polymers into microfluidic and process engineering systems is a transformative approach to autonomous process control.[1–3] Unlike conventional electromechanical actuators, these so-called smart materials convert (chemo-)physical properties from their environment directly into macroscopic volume changes.[4–6] Copolymer networks based on *N*-isopropylacrylamide (NiPAAm) and/or acrylic acid (AA) are well-established within the class of materials with smart features.[7,8] Copolymers of NiPAAm are versatile in that regard, potentially having a dual responsiveness, i.e. to temperature and pH in water. The structure of NiPAAm-AA copolymers is determined by the copolymerization conditions, the presence of crosslinkers and by the ratio of the monomers.[9–13] They have a pronounced swelling behavior with a dependence on the choice of solvents.[14–18] The potential of the NiPAAm and AA copolymers as organogels in autonomous valves for regulation of fluid flow in dependence of an organic medium is therefore of major conceptual importance in the context of reaching self-regulating reactor setups and for lab-on-a-chip applications.[19–22] The mostly soft materials come along with an inherent mechanical compliance of a swollen network, which may be incompatible with its functioning in operational technical components.[23,24] The hydrogel or organogel actuator in a typical valve configuration must be able to reversibly and repeatedly expand in a casing against a hydraulic pressure gradient in order to seal a channel.[25]

Previous studies on spherical P(NiPAAm-*co*-AA) beads have demonstrated that soft gels exhibit useful swelling ratios and fast diffusion kinetics, but that they may lack the structural integrity necessary for reliable operation.[26–28] Soft organogel beads in particular tend to deform significantly under hydrodynamic stress. The compliant material can protrude into the valve seat when used to control the flow of a fluid. This mechanical failure mode of the gel would hamper a valve from reopening, even when in particular a chemical trigger for shrinkage is present and thus impairing its function.

It thus seemed useful to find an easy method, i.e. one without performing a polymerization, for fitting the mechanical property profile of an organogel to the application as a smart component in a solvent-responsive passive valve. This challenge was met by a post-synthesis reinforcement strategy, i.e. one beyond covalent crosslinking which may give complex outcomes after change of the recipe for an NiPAAm gel synthesis. In addition, increasing the concentration of covalent crosslinkers (e.g. *N*,*N*-methylene bisacrylamide, MBA) in a resin formulation may stiffen the resulting network. Gels with a higher crosslink density may become

* *Correspondence to: GA Luinstra, Institute of Technical and Macromolecular Chemistry, University of Hamburg, Bundesstrasse 45, 20146 Hamburg, Germany. E-mail: luinstra@chemie.uni-hamburg.de*

Institute of Technical and Macromolecular Chemistry, University of Hamburg, Hamburg, Germany

brittle, will have a lower swelling capacity and the response to a change in chemical environment will be smaller and/or slower.[9,29]

The starting point of this investigation was therefore a low density crosslinked, macroporous P(NiPAAm-AA) gel. It was expected to exhibit a fast responsiveness and additionally to be susceptible to modification through the coordination of metal ions. A fast response to changes in chemical surrounding (pH) or temperature of NiPAAm copolymer-based hydrogels with a macroporous morphology is well documented.[30–35] In addition, the coordination of multivalent metal cations such as Fe^{3+}, Al^{3+} and Ca^{2+} to a P(AA) backbone's carboxylate units provides an option for a dynamic and tunable reinforcement.[36–39] The properties of a P(NiPAAm-AA) copolymer should thus be adjustable by metal ions introducing secondary dynamic interactions into the network, like the concept of, for example, dual networks and supramolecular hydrogels.[40–42] Fe(III) ions were selected for this study. Divalent calcium forms weaker ionic bridges and Fe(III) ions form multinuclear supramolecular clusters more effectively than trivalent Al(III) cations. These clusters act as multifunctional, energy-dissipating chemical crosslinking nodes. In aqueous poly(acrylic acid) (PAA) systems, Fe(III) ions are known to form strong coordination complexes and generate rigid supramolecular clusters that act as dynamic crosslinking points.[43–45] The resulting domains can dissipate energy and effectively harden the bead in its swollen state by restriction of the chain segment mobility. The color that comes along with the coordination of Fe(III) ions is also favorable to automated visual detection of volumetric changes on account of the higher contrast this offers.

Although many studies report on ionically crosslinked hydrogels in water, the application of such gels in organic reaction media (i.e. in organogels), such as ethanol or acetic acid mixtures, seems to have received little or no attention.[46] Most studies concern the macroscopic effects on hydrogels after the addition of metal ions.[47–49] A detailed analysis of such effects of ion concentration on the network in the form of structure–property relations also seems absent. This type of knowledge, however, could be valuable for an application of a modified smart gel, for example, in a valve application, which is our particular interest.

Here a post-synthetic ionic reinforcement of P(NiPAAm-*co*-AA) (OG10-10) organogel beads is carried out with the objective of reaching a smart material for organic solvent switching applications where shape retention during cycling is of paramount importance. The beads are prepared by a scalable UV-initiated droplet polymerization process which was reported previously.[28] A quantitative crosslinking involving iron(III) chloride based on ionic interactions was worked out in ethanol comprising a determination of iron uptake using a colorimetric thiocyanate assay.[49] This allowed us to map the binding efficiency of iron(III) ions and to relate this to the dynamics and extent of volume change upon a chemical trigger. The shrinkage on the change of medium from ethanol to ethyl acetate demonstrates a controllable transition from soft deformable gels to rigid, pressure-resistant beads by the iron content. The iron loading can be related to the resulting compressive strength. This approach provides a foundation in materials science for overcoming the mechanical limitations of soft actuators and paves the way for the next generation of robust, autonomous valves.

EXPERIMENTAL

Materials

AA (Synthopol Chemie, 21 614 Buxtehude, Germany), ethanol absolute ≥99.8% (VWR Chemicals, 64 295 Darmstadt, Germany), ethyl acetate (BCD Chemie GmbH, 21 079 Hamburg), iron(III) chloride hexahydrate reag. Ph. Eur. ≥99% (Sigma Aldrich, 82 024 Taufkirchen, Germany), lithium-phenyl-2,4,6-trimethyl benzoyl phosphinate (TPO-Li) ≥95% (Sigma Aldrich, 82 024 Taufkirchen, Germany), MBA ≥98% (Sigma Aldrich, 82 024 Taufkirchen, Germany), *N*-isopropyl acrylamide 97% (Thermo Scientific Chemicals) and silicone oil M 200 (Carl Roth, 76 185 Karlsruhe, Germany) were all used as received from the supplier.

Synthesis of P(NiPAAm-*co*-AA) hydrogel and organogel beads

The P(NiPAAm-*co*-AA) hydrogel beads were prepared as described before.[28] The precursor solution was prepared from 6 g of NiPAAm and 6 g of AA (20 wt% in total) in 48 mL of water (80 wt%). The crosslinker MBA (180 mg; 0.3 wt% relative to the total monomer content) and photoinitiator TPO-Li (60 mg; 0.1 wt%) were added and dissolved with vigorous stirring. The resulting mixture was degassed under atmospheric pressure by sonification for 5 min. The solution was added dropwise through polytetrafluoroethylene tubing (1.6 mm inner diameter) with a syringe pump (LongerPump Model LSP02-1B with a 20 mL HENKE-JECT syringe) using a constant flow rate of 3 mL min^{-1} to a beaker with 250 mL of silicone oil (ρ = 0.975 g cm^{-3}). The beaker was previously placed in a reflective chamber (180 × 180 × 180 mm^3) with a UV light source (Hoenle LED Cube 100 IC; irradiation intensity up to 1100 mW cm^{-2} at a wavelength of 365 nm). The hatch door of the chamber was modified to allow the tubing to pass to the inside. The tube ends just above the silicone oil. The forming droplets sink slowly to the bottom of the beaker; polymerization is essentially completed within 30 s (approximate time of sedimentation). The hydrogel beads were collected on a Büchner funnel and washed carefully with ethanol to remove the silicone oil. The collected beads were subsequently equilibrated in ethanol (3 × 100 mL for 24 h) to yield the parent organogel beads utilized for all subsequent modifications.

Determination of the solid content

A defined amount of the wet gel beads (approximately 2.0 g), equilibrated in the respective solvent, was weighed using an analytical balance after carefully removing surface liquid with filter paper. The samples were shock-frozen in liquid nitrogen and subsequently lyophilized at −90 °C and 0.250 mbar for 48 h using a Gamma 2-16 LSCplus freeze-dryer (Osterode am Harz, Germany) until a constant mass was reached. The resulting dry mass (m_{dry}) was recorded, and the solid content was calculated as the ratio of dry mass to wet mass according to the equation SC = (m_{dry}/m_{wet})·100%. For the ethanol-equilibrated beads utilized in the post-synthetic modification, a solid content of 18.64 wt% was determined.

Post-synthetic modification and quantification

Ionic crosslinking by Fe(III)

Ethanol-equilibrated beads (2.0 g wet mass) were submersed in 20 mL of ethanolic iron(III) chloride hexahydrate solution ($FeCl_3 \cdot 6H_2O$) with concentrations of 12.7 mmol L^{-1}, 42.3 mmol L^{-1} and 127.0 mmol L^{-1} (corresponding to molar feed ratios of Fe^{3+} to carboxylic acid groups of 0.1:1, 0.33:1 and 1:1, respectively). The mixtures were agitated on an orbital shaker in the dark for 48 h. The beads were collected on a frit and washed with 150 mL of ethanol, with a contact time of about 5 min. This washing procedure was repeated until the supernatant remained visibly colorless, and then repeated one more time, usually adding up to five cycles.

Colorimetric determination of Fe(III) loading

A solution of potassium thiocyanate in ethanol (5 g in 100 mL) was prepared and 300 µL of the supernatant of the iron crosslinking solution after the 48 h of equilibration was added for the lowest and medium concentrations of Fe(III), and 50 µL for the highest concentration. A UV–visible spectrophotometer was used to record the absorbance at a wavelength of 496 nm, corresponding to the maximum of the formed iron(III) thiocyanate complex (Supporting Information, Fig. S1, Table S1). A linear calibration curve was established using Fe(III) solutions with concentrations ranging from 0.015 to 0.100 mmol L^{-1} (Fig. S2). The solvent matrix of these calibration standards was matched to the samples using ethanol. The limit of detection and the limit of quantification for this colorimetric assay were determined to be 0.0009 mmol L^{-1} and 0.0027 mmol L^{-1}, respectively. The dilution factors of 1:333 and 1:2000 of lowest/medium and highest iron concentration of the supernatant, respectively, ensured that the absorbance values fell within the linear calibration range. The calculation of the mass-specific iron loading q (mmol g^{-1}) was based on the molar consumption of iron ions (Δc), the solution volume (V) and the dry mass of the polymer (m_{dry}).

Volumetric tracking of the swelling behavior by inline monitoring

Volumetric dimensional changes and swelling behavior were monitored at 25 °C using an *in situ* optical tracking setup as described previously.[28] The organogel beads were fixed on a thin metal skewer inside a 100 mL glass cuvette that was sealed with a custom-made 3D-printed lid to prevent solvent evaporation. Image sequences were recorded at defined intervals (every 30 s) using a digital camera (Canon EOS R50). Data evaluation was performed using a custom-developed Python script based on computer vision algorithms. Unlike previous studies on transparent gels, the iron-loaded beads exhibited a distinct deep orange coloration. The software utilized this specific feature to detect the beads against the black background using color thresholding. After isolating the region of interest, the bead diameter was determined via contour detection. The resulting pixel values were converted into metric dimensions using a calibration scale to calculate the radius and volume. The beads remained round during swelling/shrinkage. Swelling/shrinkage cycles were performed in duplicate ($n = 2$); the experiments were very reproducible.

Characterization

UV–visible spectroscopy

UV–visible spectroscopic measurements were performed on an Agilent (Santa Clara, CA, USA) Cary 60 with a xenon flash lamp (80 Hz) as light source. The measurements were performed over a wavelength range of 300–600 nm with a scanning rate of 600 nm min^{-1}.

Fourier transform infrared (FTIR) spectroscopy

Attenuated total reflection FTIR spectra of the samples were recorded using a Shimadzu IR Spirit with QATR-S (Unit Shimadzu Deutschland GmbH, Duisburg, Germany). The measurements (average of 15 scans) were conducted over a spectral range of 4000–400 cm^{-1} with a resolution of 2 cm^{-1}.

Morphological characterization

Morphological evaluation of the gel networks was achieved after generation of a hydrogel, freezing in liquid nitrogen and then lyophilization at −90 °C and 0.250 mbar for 48 h (Gamma 2–16 LSCplus, Osterode am Harz, Germany). The Fe-modified organogels were transformed to the corresponding hydrogels by immersing in water for 48 h. This was a technical necessity as the freeze-dryer reaches a minimum temperature of −90 °C, which is too high for freezing ethanol at a minimum of −114 °C. Evaporating liquid ethanol from the organogels during lyophilization would generate high capillary forces, which would impair the porous network. The lyophilized beads were removed from water and bisected through their center using a sharp scalpel. They were subsequently sputter-coated with a thin Pt layer. The analysis was performed at an accelerating voltage of 5 kV (LEO Electron Microscopy Inc., One Zeiss Drive, Thornwood, NY 10594, USA) and a duration of 328 s at a resolution of 138 eV and a take-off angle of 7.87°. The software SmartSEM V06.00 was utilized to analyze SEM images and TEAM was used for the energy-dispersive X-ray spectroscopy (EDX) measurements.

Flame atomic absorption spectrometry

The total iron content was determined using flame atomic absorption spectroscopy (F-AAS) on a Solaar S Series spectrometer (Thermo Fisher Scientific) equipped with an autosampler. Therefore, an exact amount of organogel (ethanol swollen) beads were subjected to microwave-assisted acid digestion (5 mL of inverse aqua regia (HNO_3/HCl, 3:1 v/v) at 250 °C using a microwave digestion system by Anton Paar). The resulting solutions were then diluted to a final volume of 15 mL. The samples were further diluted on demand for the F-AAS measurements to fall within the calibration range. Atomization was performed in an air/acetylene flame, with an iron hollow cathode lamp acting as the light source. The device was calibrated using a five-point calibration within the concentration range of 0.50–2.50 mg L^{-1} (0.50, 1.00, 1.50, 2.00 and 2.50 mg L^{-1}). All measurements of the standards and samples are triplicate determinations; the mean value is given. The limits of detection and quantification for iron were 0.0923 and 0.341 mg L^{-1}, respectively.

Mechanical characterization

Testing was on beads that were fully equilibrated in ethanol. Individual swollen beads were removed from the solvent and immediately placed in the center of the lower plate. All measurements were conducted at ambient conditions in a climatized room. Uniaxial compression tests on individual organogel beads were performed on a Discovery HR-2 hybrid rheometer (TA Instruments, New Castle, DE, USA). The rheometer was equipped with a 25 mm parallel plate geometry made of steel (ETC Steel, item no. 453606.901). The measurements were performed at a controlled temperature of 25 °C using the Peltier plate system. The individual beads were placed in the middle of the lower plate. Compression was performed in the standard motor direction at a constant linear rate of 50 µm s^{-1} over a period of 200 s. The compression modulus (E) was calculated from the linear elastic range of the force–deformation curves (up to 10% strain) using Hertz's theory for the contact of a sphere with a rigid plane. The evaluation uses the Hertz contact model for the initial compression range with the relationship between the applied force (F) and the displacement (δ) following the equation[50,51] $F = \frac{4}{3}\frac{E}{1-\nu^2}\sqrt{R\delta^3}$ with R as the radius of the undeformed bead and ν as the Poisson ratio: a value of 0.5 was taken for ν because of the inherent incompressibility of the organogel network.[52] Regression analysis of the experimental data within the first 10% of strain yields the Young's modulus for each sample. All test results are the average of three determinations (n of 3).

RESULTS AND DISCUSSION

Round beads consisting of copolymers of NiPAAm and AA (1 to 1 in weight) were prepared as described before in water (section entitled Synthesis of P(NiPAAm-*co*-AA) hydrogel and organogel beads).[28] The beads are macroporous with pores in the range 4–5 µm. They were conditioned in ethanol to reach the parent organogel beads with about 7 mm diameter in the equilibrated state.

Post-synthesis ionic crosslinking

The parent beads were modified by incorporating iron(III) ions into the network. They were therefore immersed in $FeCl_3{\cdot}6H_2O$ containing ethanolic solution for 48 h. Aliquots of such solutions with various concentrations were used to target specific molar ratios of the iron ions to the carboxylic acid groups of the copolymeric beads (ratio of n_{Fe} to n_{COOH}). The uptake of iron(III) ions was determined spectroscopically from the residual concentration in the supernatant and by elemental analysis of the beads (Tables 1 and S2).

The beads shift from a white-opaque appearance to an orange color upon contact with the iron(III) solution (Fig. 1). The opacity of the beads was retained and appears intensified as the beads are more reflective. This already hints that the introduction of ionic crosslinks further increases the density of the polymer network domains.

The organogel beads were modified with up to stoichiometric amounts of iron(III) ions with respect to the amount of carboxylic acid entities in the beads. Three modifications were taken into consideration, i.e. beads with a low, a medium and a high loading were prepared (Table 1). The samples are labeled accordingly. It is not known what type of ionic crosslinks would arise and what average stoichiometry results for the reaction of iron(III) chloride with potential amide, carboxylic acid and carboxylate ligands at the polymer backbone (next to water and ethanol of the solvent).

The experiment leading to Fe-Low exhibited a near-quantitative depletion of iron(III) in the supernatant (>99% efficiency), yielding a loading q of 0.67 mmol g^{-1}. This indicates a high binding affinity of the carboxylic acid entities in the ethanol swollen state of the beads. Concomitantly, a test with wet indicator paper gave a response equal to an aqueous solution with pH 2–3 immediately after contact with the supernatant (the parent ethanolic iron(III) solution shows an equivalent pH value of 3–4). This is an indication that the protons on the carboxylic acids of the copolymer are replaced by iron(III) ions. Possibly, an equilibrium is established for the exchange in ethanol; this, however, was not investigated.

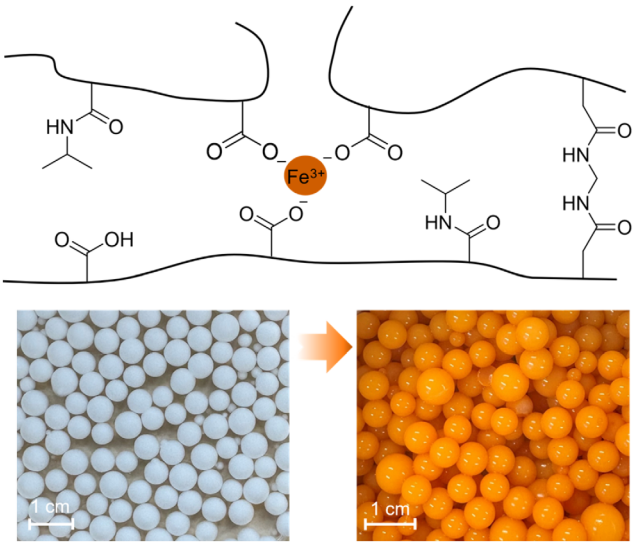

Figure 1. Tridentate Fe-carboxylate coordination motif and the macroscopic appearance of the opaque reference beads before (left) and after (right) 48 h of loading.

Elemental analysis of the isolated, dried Fe-Low beads and the Fe-Mid sample yielded results comparable to those obtained by spectroscopic analysis. Only the iron content of the Fe-High sample is significantly lower by elemental analysis than is calculated from the change of its concentration in the supernatant. The differences are associated with the sample preparation of the ethanol-swollen beads which will lose some ethanol from the pores. The affinity of the beads for iron(III) ions obviously is limited as the supernatant is not depleted to a similar extent as for Fe-Low, neither in the case of the Fe-Mid nor of the Fe-High preparations. The steric constraints of the network will limit the number of sites for iron ion binding, and the concentration of formally hydrochloric acid in the supernatant increases with iron(III) ions reacting with the beads' carboxylic acid entities. Similar chemistry is found for PAA.[49] Acetic acid in ethanol is reported to react with $FeCl_3{\cdot}6H_2O$ to yield hydrochloric acid ($FeCl_3.6H_2O$/EtOH + –COOH → HCl + '$FeCl_2$'-(COO)).[53] The P(NiPAAm-AA) copolymer has weak basic entities in the form of the *n*-isopropyl amide that can assist in the deprotonation of the acid yielding the corresponding carboxylate anion. Indeed, the reaction between isobutyric acid (mimic for PAA) and $FeCl_3{\cdot}6H_2O$ in ethanol with NiPAAm readily gives a change in the coordination of the iron center (Fig. S3).

Table 1. Organogels after treatment with iron(III) solution

ID	Feed c (mmol L^{-1})	Fe:$COOH_{feed}$ (mol:mol)	Depletion Δc (mmol L^{-1})	Fe:$COOH_{bead}$ (mol:mol)	Yield Fe^{3+} (%)	Loading[S] (mg Fe g^{-1})[a]	Loading[EA] (mg Fe g^{-1})[a]
Fe-Low	12.7	1:10	12.5	1:10	99	37.5	33.9 (0.7)
Fe-Mid	42.3	1:3	23.1	1:5.6	55	69.2	68.2 (0.7)
Fe-High	127.0	1:1	33.8	1:3.8	27	101.6	85.5 (1.6)

Note: Post-synthesis ethanol swollen beads were treated with 20 mL of ethanolic iron(III) solution. The iron loading is reported per gram of beads taken from the solution and shortly dried in air to remove surface ethanol (some ethanol may have evaporated from pores of the bead during sample preparation).
[S] By spectroscopy (single measurements).
[EA] By elemental analysis.
[a] mg Fe g^{-1} refers to weight of iron per gram of ethanol-swollen beads.

The FTIR spectra of the parent organogel (OG10-10) and the iron-saturated hybrid (Fe-High) differ in particular in the bands that are associated with the carboxylic acid entities. The spectrum of the unmodified bead has prominent features at 1730 cm^{-1} and 1250 cm^{-1} (Fig. 2). These are related to the C=O stretching vibration of the protonated carboxylic acid groups (–COOH) derived from AA comonomer. These bands are still present in the spectra of Fe-High but with a much lower intensity. New bands appear in the lower wavenumber range at 1540–1580 cm^{-1} and 1400–1450 cm^{-1}. These can be attributed to the asymmetric ν_{as} and symmetric ν_s stretching vibrations of the carboxylate anion (COO^-) coordinated to a metal center.[54,55] The presence of these specific carboxylate modes, combined with the decreased intensity of the free acid absorption band, provides direct evidence that the iron ions are chemically bound to the polymer backbone by carboxylate coordination, rather than physically trapped in the gel network. This is consistent with the lowering of the pH value of the supernatant solution.[49]

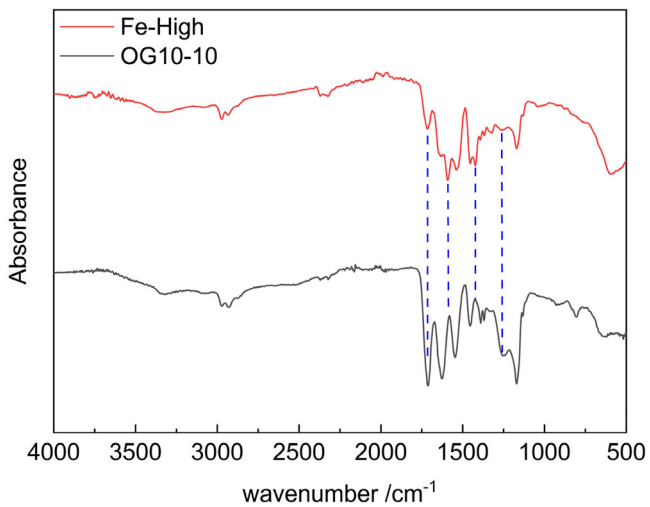

Figure 2. FTIR spectra of OG10-10 and Fe-High gel.

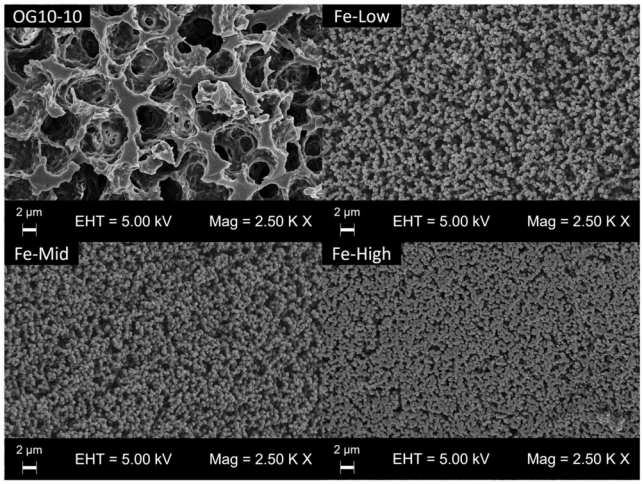

Figure 3. SEM images of freeze-dried virgin (OG10-10) and iron(III) ion-treated beads after freeze-drying from water (Table 1).

Morphological evolution and microstructure

The diameter of the beads in ethanol is about 15% smaller in magnitude after the reaction with iron(III) ions. This is almost independent of the amount of iron(III) ions that ends up in the bead. This observation is in accord with the early formation of an iron(III) ion crosslinked outer shell, which probably is also of importance for the consecutive crosslinking (*vide infra*). The original polymer network seems to collapse upon iron ion incorporation as also can be deduced from SEM images (Fig. 3). The microscopic images are of freeze-dried samples of the corresponding hydrogels. The Fe-organogel beads were immersed in water for 48 h to generate the hydrogel analogs. A reconditioning in ethanol did not give evidence for a change in the structure. An Fe-Low bead had very similar kinetics for shrinkage and swelling in ethyl acetate and ethanol, respectively, and also the time-dependent curve followed that of Fe-Low closely (Fig. S4, *vide infra*). The conditioning in water does not fundamentally change the beads.

The drying process in the preparation for SEM imaging inevitably stresses the soft hydrogel structure and alters the dimensions of the solvent-swollen pores. A uniform preparation may at least preserve differences to capture the permanent structural microsyneresis induced by the iron coordination. The image of the parent beads shows the macroreticular architecture with larger open pores and channels. The morphology features a sponge-like structure with interconnected cavities. This structure results from phase separation during the photopolymerization process.[13] The open porosity also facilitates the rapid initial diffusion of metal ions into the matrix.

The coordination of the carboxylate groups to iron(III) triggers the collapse to a continuous network of densely packed, more globular domains. This granular morphology indicates strong local compaction (microsyneresis) of the polymer chain segments by coordination to Fe(III) ions.[56] The Fe-Low samples seem to have distinguishable, spherical agglomerates with visible interstitial boundaries. At higher iron concentrations (Fe-Mid and Fe-High), however, the agglomerates merge more and more into a situation with a compacted surface layer. The surface agglomerates show a similar size for iron(III) modified beads of approximately 0.25 µm, but become more compressed as the iron(III) content increases.

Intraparticle iron distribution

EDX analysis of bisected beads shows that the iron ions are absorbed non-uniformly over the radius of the beads in the 48 h of exposure, which is in particular noticeable from imaging of Fe-Low: its beads have a pronounced core–shell structure. EDX mapping shows a brighter signal intensity at the surface of the beads, leaving the core dark (Fig. 4(a)). Quantitative analysis of defined 50 × 50 μm^2 areas confirms this steep gradient. The outer shell measurement gives an iron concentration of 3.57 wt%, contrasting to an almost negligible content of 0.37 wt% in the particle center.

It is inferred that a rapid complexation of the available iron ions (1 for any 10 carboxylic acid entities) at the interface between liquid and solid consumes the limited starting material before significant diffusion into the mass can take place. Consequently, the number of iron ions in the supernatant solution is used up before the core can be reached. This also indicates that the mobility of the iron(III) ions is low once they are bonded in the copolymer. This kind of structure formation is of course of high relevance for both the mechanical and the swelling properties. It may more readily form in a post-synthesis modification than in a direct synthesis.

Polymer International published by John Wiley & Sons Ltd on behalf of Society of Chemical Industry.

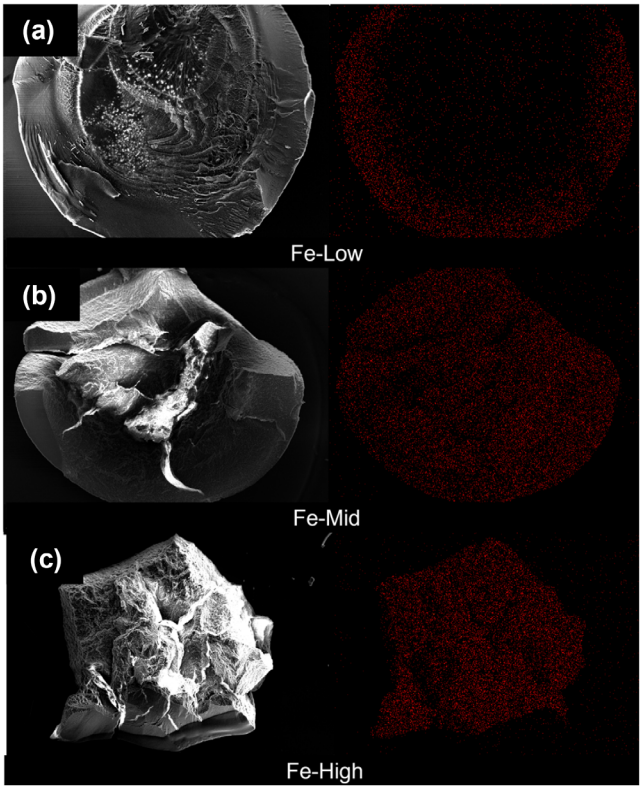

Figure 4. Cross-sectional SEM images (left) and EDX mapping (right; red dots indicate the presence of iron) of the Fe-gel beads: (a) Fe-Low, (b) Fe-Mid and (c) Fe-High samples.

The Fe-Mid (1 Fe(III) per 3 COOH in the feed) and Fe-High (1 Fe(-III) per 1 COOH) beads show a more homogeneous distribution of the iron ions over the diameter (Fig. 4(b), (c)). The number of iron ions in the feed solution are now sufficient to reach the center of the bead. The intermediate surface functionalization is not preventing the cations from diffusing into the bead in the 48 h of exposure: the iron ions appear distributed evenly over the surface of the bead, i.e. as deep as the EDX analysis detects iron ions on the bisected beads. This structural difference has a direct impact on the appearance: unlike the Fe-High beads, the Fe-Low beads remain soft.

Mechanical properties and responsiveness

Mechanical characterization

The coordination of iron(III) ions causes a mechanical reinforcement of the polymer network. Force–compression analysis demonstrates the transition of a compliant, soft organogel swollen in ethanol from its synthesis to a rigid, hard organogel bead characteristic for Fe-High. This is reflected in the Young's moduli of the ethanol-swollen beads at low compression and generally in their compression–force dependences at higher deformation (Table 2; Fig. 5). The latter is of more importance for applications where changes larger than 10% will be relevant. The elastic moduli, determined using the Hertzian method of evaluation at small compressions, indicates improvements in the stiffness of almost one order of magnitude for Fe-Low to over two for Fe-High (relative to the parent OG10-10 bead). The value of Fe-High of 2.3 MPa is about an order of magnitude higher than of a comparable hydrogel crosslinked with $Fe_2(SO_4)_3$ (determined in extension).[49] The values for the Fe-Low beads compare well

Table 2. Mechanical properties of the beads from compression measurements

Sample	Young's modulus[a] (kPa)	Improvement to OG10-10	Force at 30% compression (N)
OG10-10	6.1		0.03
Fe-Low	47	~8×	0.38
Fe-Mid	910	~152×	7.3
Fe-High	2300	~378×	15

[a] Derived from the Hertzian slope k of the compression curves ($F \propto \delta^{1.5}$) at compression less than 10%.

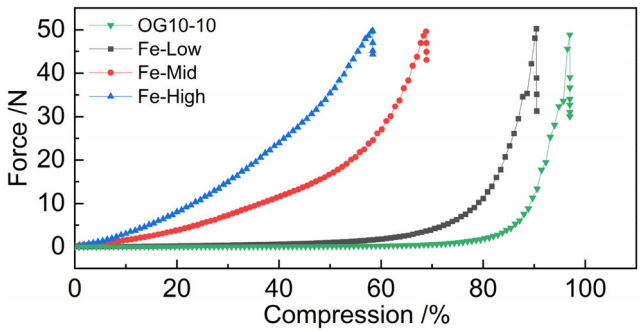

Figure 5. Compression curves of single beads.

to a photopolymerized PNiPAAm with 4 wt% of MBA as crosslinker (81 kPa).[57]

All of the beads of this study can withstand forces of over 40 N at a terminal compaction, but the path to this situation differs markedly. The OG10-10 beads require compression of over 95% to build up significant resistance (Fig. 5). In contrast, the Fe-High beads show an immediate increase in resistance to compression to reach the 40 N threshold at a compression of only 54%. A network has formed that restricts the mobility of the polymer chains even under moderate deformation.

The force required for 30% deformation illustrates the tunability of the bead mechanics with the amount of iron(III) ions. Compression of the beads Fe-High (15 N) needs approximately 500 times the force of the OG10-10 sample (0.03 N) and 40 times the force of Fe-Low (0.38 N). The force necessary for 30% compression increases linearly with the iron concentration in the range Fe-Low to Fe-High. The stiffness of the network increases by several orders of magnitude for higher loadings, reaching 0.91 MPa for Fe-Mid and 2.3 MPa for Fe-High (i.e. following a power law with exponent close to 4 with respect to the iron content). A structural interpretation is not attempted considering the non-simple structure of the modified beads. It is clear, however, that a response of the beads involving a change of volume would be expected to follow the trend in mechanical properties.

Degree of swelling in ethanol and ethyl acetate

The usefulness of organogels as active smart components is of course very much dependent on their capacity for reversible volume changes. The modification of the parent OG10-10 gel with iron(III) ions retains the copolymeric beads as smart materials (Fig. 6). The alternating solvent conditions ethyl acetate–ethanol at 25 °C reveal also the trade-off between mechanical stability

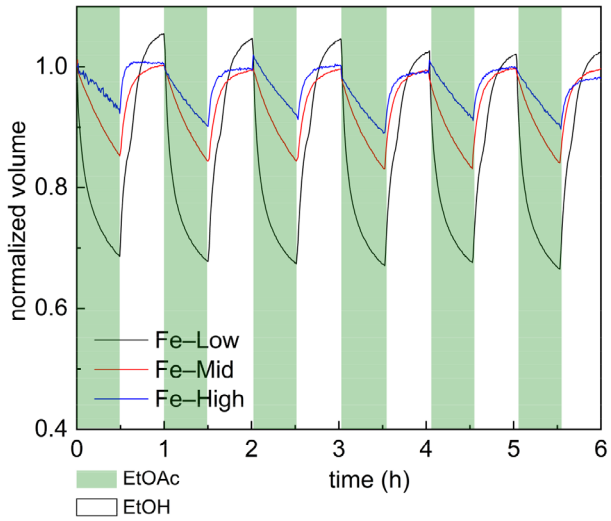

Figure 6. Volume-normalized dynamic swelling and shrinking of the Fe-modified gels (right) under cyclic solvent exchange at 25 °C from EtOAc (green underlay) to EtOH.

and reversibility. The Fe-High beads are mechanically the most robust but have also the smallest change of volume. The optimum composition for a bead will be dependent on the specific application with its necessary degree of response and robustness in flow applications. The responsivity of the beads was addressed in detail by an analysis of the degree of swelling in ethanol and ethyl acetate and from the kinetics of shrinkage and swelling during cyclic exposure to them.

The cyclic exposure of the beads to ethanol and ethyl acetate leads to very similar responses over time, indicating the beads are not decomposing. The chemical stability of the hybrid network was addressed by testing the solvents for leached iron ions using the sensitive colorimetric potassium thiocyanate (KSCN) test and subsequent UV–visible spectroscopic detection. No absorption was detected at 496 nm; the concentration of free Fe^{3+} ions remains below the detection limit. This confirms that the metal centers are, within the time frame of the experiment, effectively irreversibly coordinated in the polymer matrix and are not released during the volume phase transitions in ethanol–ethyl acetate. This is consistent with the observed formation of a persistent core–shell morphology.

As noted above, the size of the beads in ethyl acetate, i.e. after a solvent exchange from the ethanol of their synthesis, is larger the greater the amount of iron(III) ions, i.e. the responsiveness for the specific exchange becomes smaller at high iron(III) ion loadings (Fig. 6; Table 3). The dynamic swelling properties and cononsolvency behavior of the parent system were described in detail before (Fig. S5).[28] The ethanol swollen OG10-10 bead will shrink when placed in ethyl acetate. The time-dependent shrinkage appears to have two phases, which can be described by two exponentials; the one with the smaller time constant will be relevant for the longer second phase.[58] The first phase goes along with larger changes of volume, which can be approximated by an exponential decay of the diameter (Table 3).[59,60] The consecutive reswelling in ethanol will proceed with an intermediate shrinkage which is followed by also an exponential swelling.

The alternate exposure of the iron(III) modified beads for 30 min to ethanol and ethyl acetate leads to a similar shrinkage–swelling response (Fig. 6). However, swelling of the modified beads in ethanol (from ethyl acetate) does not proceed with a prominent transient deswelling anymore; only for Fe-Low does the volume increase still show a small intermediate deceleration. This is a reproducible feature and is to be related to the cononsolvency of the beads in ethanol–ethyl acetate mixtures (minimum volume at a respective vol:vol ratio of 1:4).[28] The less-crosslinked gel Fe-Low with the tentatively more or less unchanged core behaves more like the parent gel.

The extent of relative shrinkage of the beads' volume is largest for Fe-Low; it is even larger than that of the parent OG10-10. Apparently, a more compact structure can form in ethyl acetate, the presence of iron being favorable in low amounts. It is known that the OG10-10 beads will shrink to a higher degree on account of the presence of residual ethanol, i.e. in ethyl acetate:ethanol mixtures up to a volume ratio of 4:1.[28] It is currently not known whether both phenomena are related for reaching a more dense structure. The larger difference between swelling and shrinkage of Fe-Low is favorable for a smart application.

The two-step shrinkage process of the diameter of parent OG10-10 turns into a smoother decrease of the volume, the more iron is present in the polymer. A fast first phase again is recognizable in the shrinkage of Fe-Low and it proceeds for a longer time;

Table 3. Ethanol–ethyl acetate exchange response of beads at 25 °C

Sample	OG10-10	Fe-Low	Fe-Mid	Fe-High
Initial diameter (cm)	0.7	0.61	0.6	0.6
Max loss of diameter[a] (%)	11	15	10	9
Max loss of volume[a] (%)	30	38	26	25
Loss of volume at 30 min[a] (%)	30	36	17	11
Kinetics of shrinkage				
Duration first phase[b] (s)	120	270	30	30
Time constant (1000 s)	0.40 (0.01)	0.80 (0.05)	1.8 (0.4)[c]	3.3[c] (0.4)
Kinetics of swelling				
Time constant (1000 s)	0.30 (0.01)[d]	0.34 (0.01)[d]	0.36 (0.01)	0.31 (0.02)

[a] Calculated from the exponential decay; standard deviation smaller than 1%.
[b] Estimated from the shrinkage, deviation of <30 s.
[c] First cycle not included (outlier 1/3 of the value, the bead relaxes after its synthesis).
[d] After the intermediate swelling–shrinkage.

in Fe-Mid and Fe-High it is reduced to one data point (30 s; Table 3). It is tempting to relate this to smaller pores/channels in the iron(III)-crosslinked beads (Fig. 3) with a lower effective diffusion.[32] The fast first phase of ethanol diffusion out of the bead into the bulk ethyl acetate becomes slower, presumably without much change inside the polymer segments.[18,61] The polymer segments of the bead can only react to a change after they have contact with the new medium.[31] The diffusion time for ethanol or ethyl acetate over a length to 0.3 cm is in the range of 10^3 s, making the mass transfer part of the rate-determining step for changes in the bead polymer structure (which only makes up 10%–20% of the mass).

The longer, second phase of the shrinkage of the ethanol swollen beads in ethyl acetate can be fitted in terms of the diameter d to an exponential decay function $d(t) = A + B\exp(-t/\tau)$ (Table 3; Fig. S6). This allows a time constant to be extracted which can be used for a comparison of rates. Six cycles were evaluated individually and the values for A and τ were averaged (Table 3; Supporting Information). The standard deviation for the values of A is below 3%, making the extent of the response very predictable. The standard deviations for values of the time constant τ of the responses of in particular the shrinkage in ethyl acetate are larger; the differences between the beads remain significant (Table 3). It is noted that, only for Fe-High and Fe-Mid beads, larger spreads for values of τ were found in the first cycles of swelling; these were omitted in the analysis as outliers (Fig. S5). It may be that the gel beads undergo a small change in their constitution; the behavior becomes very predictable thereafter. A relaxation of the structure is not uncommon; measurements of the behavior were started thereafter.[62] Note that the time of 30 min is not enough to reach that maximum shrinkage for Fe-Mid and Fe-High. The observed values for the loss of volume in ethyl acetate within the 30 min of the cycling is therefore also given. A significant enough change of volume (>10%) for application in a valve is given within the 30 min.

The rate of shrinkage of the ethanol-saturated beads after placement in ethyl acetate decreases strongly with the iron content. The time constant increases from 800 s for Fe-Low to about 1 h for Fe-High, making the latter unattractive as a valve component.

The swelling of the iron(III) modified beads in ethanol follows a similar exponential with a time constant between 300 and 360 s (Table 3). The differences are small, however, and an interpretation in terms of the crosslinking which should also encompass the difference in the magnitude of the response cannot be reasonably made at this time. The segments/domains of the copolymer move into the ethanol bulk while ethyl acetate in the inner part is replaced. The effective rate will be dependent on the diffusion of ethanol and secondarily on the elastic properties of the gel.[60] The difference in the dependence of the shrinkage and swelling on the iron(III) content shows again that shrinkage and swelling are fundamentally different processes.[60]

CONCLUSIONS

This study demonstrates that post-synthetic ionic coordination is an effective method for overcoming the fundamental limitation in mechanical compliance of soft organogel actuators without relying on carbon–carbon bond formation. The study establishes a direct link between diffusion control during loading and the resulting functional morphology. The architecture can be adjusted to create either a heterogeneous core–shell structure for high responsiveness with moderate hardening or a more homogeneous network for maximum compressive strength. The generation of a more robust shell with flexible domains, which is not readily achieved in a one-step synthesis, is a good option for reaching a material with still a good responsiveness and acceptable time constants for reversible swelling–shrinkage operations. This is demonstrated by the near-disappearance of the intermediate shrinkage during swelling in ethanol of the ethyl acetate swollen state in the reinforced beads: the mechanical locking of the polymer chains by the iron(III) ion crosslinks slows the intermediate shrinkage down, until it disappears at the level of Fe-Mid. In terms of applications in fluidic systems, the Fe-Low bead has options as a sensitive chemical sensor and a robust actuator. The combination of chemical stability, adjustable hardness and the ability to mechanically suppress thermodynamic instabilities would make these hybrid gels more reliable components for autonomous valves, an application in which parent copolymers previously failed because of their softness.

ACKNOWLEDGEMENT

Open Access funding enabled and organized by Projekt DEAL.

CONFLICT OF INTEREST

The authors declare no conflict of interest.

FUNDING INFORMATION

This project is funded by the Deutsche Forschungs gemeinschaft (DFG, German Research Foundation) – SFB 1615-503850735 (SonderForschungsBereich 1615).

SUPPORTING INFORMATION

Supporting information may be found in the online version of this article.

REFERENCES

1 Dong L and Jiang H, *Soft Matter* **3**:1223–1230 (2007). https://doi.org/10.1039/b706563a.
2 Hilber W, *Appl Phys A* **122**:751 (2016). https://doi.org/10.1007/s00339-016-0258-6.
3 Alexandre-Franco MF, Kouider R, Kassir Al-Karany R, Cuerda-Correa EM and Al-Kassir A, *Micromachines (Basel)* **15**:1137 (2024). https://doi.org/10.3390/mi15091137.
4 Zheng Q, Xu C, Jiang Z, Zhu M, Chen C and Fu F, *Front Chem* **9**:650358 (2021). https://doi.org/10.3389/fchem.2021.650358.
5 Zhu QL, Dai CF, Wagner D, Daab M, Hong W, Breu J *et al.*, *Adv Mater* **32**: e2005567 (2020). https://doi.org/10.1002/adma.202005567.
6 Kim YS, Liu M, Ishida Y, Ebina Y, Osada M, Sasaki T *et al.*, *Nat Mater* **14**: 1002–1007 (2015). https://doi.org/10.1038/nmat4363.
7 Lanzalaco S, Mingot J, Torras J, Alemán C and Armelin E, *Adv Eng Mater* **25**:2201303 (2023). https://doi.org/10.1002/adem.202201303.
8 Begum R, Farooqi ZH and Khan SR, *Int J Polym Mater Polym Biomater* **65**: 841–852 (2016). https://doi.org/10.1080/00914037.2016.1180607.
9 Da Silva R and Ganzarolli de Oliveira M, *Polymer* **48**:4114–4122 (2007). https://doi.org/10.1016/j.polymer.2007.05.010.
10 Pagonis K and Bokias G, *Polym Bull* **58**:289–294 (2007). https://doi.org/10.1007/s00289-006-0617-0.
11 Suzuki T, Ikkai F and Shibayama M, *Macromolecules* **40**:2509–2514 (2007). https://doi.org/10.1021/ma062448b.
12 Chen J, Pei Y, Yang L-M, Shi L-L and Luo H-J, *Macromol Symp* **225**:103–112 (2005). https://doi.org/10.1002/masy.200550709.
13 Xiao XC, *Express Polym Lett* **1**:232–235 (2007). https://doi.org/10.3144/expresspolymlett.2007.35.

14 Zhang W-J, Yan Y-Z, Nagappan S, He S, Ha C-S and Jin Y-S, *J Macromol Sci A Pure Appl Chem* **58**:860–871 (2021). https://doi.org/10.1080/10601325.2021.1964368.
15 Yao G, Li S, Xu J and Liu H, *J Chem Eng Data* **64**:4054–4065 (2019). https://doi.org/10.1021/acs.jced.9b00408.
16 Jin X, Wang Q, Sun J, Panezai H, Bai S and Wu X, *Int J Polym Mater Polym Biomat* **68**:463–471 (2019). https://doi.org/10.1080/00914037.2018.1466132.
17 Jin X, Wang Q, Sun J, Panezail H, Wu X and Bai S, *Polym Bull* **74**:3619–3638 (2017). https://doi.org/10.1007/s00289-017-1915-4.
18 Eckert KM, Müller S, Luinstra GA and Smirnova I, *Fluid Phase Equil* **586**:114182 (2024). https://doi.org/10.1016/j.fluid.2024.114182.
19 Schneider H-J, *Chemoresponsive Materials: Stimulation by Chemical and Biological Signals*. Royal Society of Chemistry, Cambridge (2015).
20 Wang J, Chen Z, Mauk M, Hong K-S, Li M, Yang S *et al*., *Biomed Microdevices* **7**:313–322 (2005). https://doi.org/10.1007/s10544-005-6073-z.
21 Chung T, Choi J, Enomoto T, Park S, Kim S and Kim YS, *Chem Rev* **125**:9053–9088 (2025). https://doi.org/10.1021/acs.chemrev.5c00358.
22 Yoshida R and Ueki T, *NPG Asia Mater* **6**:e107 (2014). https://doi.org/10.1038/am.2014.32.
23 Isomoto Oka Y, Sakohara S, Gotoh T, Iizawa T, Okamoto K and Doi H, *Polym J* **36**:59–63 (2004). https://doi.org/10.1295/polymj.36.59.
24 Xu L, Fu Y, Wagner RJ, Zou X, He Q, Li T *et al*., *Macromol Rapid Commun* **43**:e2200320 (2022). https://doi.org/10.1002/marc.202200320.
25 Romero MR, Arrua RD, Alvarez Igarzabal CI and Hilder EF, *Sens Actuators B Chem* **188**:176–184 (2013). https://doi.org/10.1016/j.snb.2013.06.086.
26 Pan Z, Huang Y, Guo H, Huang T, Wen G, Yu H *et al*., *Polym Adv Technol* **33**:235–245 (2022). https://doi.org/10.1002/pat.5509.
27 Gupta NV and Shivakumar HG, *J Pharm Res* **11**:481–493 (2012).
28 Gmeiner J, Hasse J, Luinstra GA et al., *Macromolecules* **59**:8403–8419 (2026).
29 Ks S, Rout S and Jacob AR, *J Chem Phys* **162**:184903 (2025). https://doi.org/10.1063/5.0269885.
30 Wang X, Dai Q, Zhong H, Liu X and Ren J, *Biores* **14**:8543–8558 (2019). https://doi.org/10.15376/biores.14.4.8543-8558.
31 Gehrke SH, Synthesis, equilibrium swelling, kinetics, permeability and applications of environmentally responsive gels, in *Responsive Gels: Volume Transitions II*, Vol. **110**, ed. by Dušek K. Springer-Verlag, Berlin/Heidelberg, pp. 81–144 (1993).
32 Alsaid Y, Wu S, Wu D, Du Y, Shi L, Khodambashi R *et al*., *Adv Mater* **33**:e2008235 (2021). https://doi.org/10.1002/adma.202008235.
33 Chung T, Im Han K, Han J, Ahn K and Kim YS, *Gels* **7**:18 (2021). https://doi.org/10.3390/gels7010018.
34 Maeda S, Kato T, Kogure H and Hosoya N, *Appl Phys Lett* **106**:171909 (2015). https://doi.org/10.1063/1.4919585.
35 Strachotová B, Strachota A, Uchman M, Šlouf M, Brus J, Pleštil J *et al*., *Polymer* **48**:1471–1482 (2007). https://doi.org/10.1016/j.polymer.2007.01.042.
36 Zhang Z, Wang X, Liu T, Liu L, Yu C, Tian Y *et al*., *Mater Des* **214**:110390 (2022). https://doi.org/10.1016/j.matdes.2022.110390.
37 Mikula K, Skrzypczak D, Ligas B and Witek-Krowiak A, *SN Appl Sci* **1**:643 (2019). https://doi.org/10.1007/s42452-019-0657-3.
38 Sarker M, Izadifar M, Schreyer D and Chen X, *J Biomater Sci Polym Ed* **29**:1126–1154 (2018). https://doi.org/10.1080/09205063.2018.1433420.
39 Kang M, Cheng Y, Hu Y, Ding H, Yang H, Wei Y *et al*., *Front Mater Sci* **17**:230655 (2023). https://doi.org/10.1007/s11706-023-0655-7.
40 Jiang H, Yang H, Wang R, Li H, Zhang S, Peng L *et al*., *Colloids Surf A Physicochem Eng Asp* **730**:139047 (2026). https://doi.org/10.1016/j.colsurfa.2025.139047.
41 Huang G, Wang P, Cai Y, Jiang K and Li H, *J Polym Sci* **61**:1675–1687 (2023). https://doi.org/10.1002/pol.20230082.
42 Ahmadi M and Seiffert S, *J Polym Sci* **58**:330–342 (2020). https://doi.org/10.1002/pol.20190076.
43 Wang X, Zheng Y, Zhang C and Chen C, *Polym Bull* **83**:45 (2026). https://doi.org/10.1007/s00289-025-06182-8.
44 Li X, Wang H, Li D, Long S, Zhang G and Wu Z, *ACS Appl Mater Interfaces* **10**:31198–31207 (2018). https://doi.org/10.1021/acsami.8b13038.
45 Li X, Zhang Y, Yang Q, Li D, Zhang G and Long S, *Iran Polym J* **27**:829–840 (2018). https://doi.org/10.1007/s13726-018-0657-y.
46 Zoumpanioti M, Merianou E, Karandreas T, Stamatis H and Xenakis A, *Biotechnol Lett* **32**:1457–1462 (2010). https://doi.org/10.1007/s10529-010-0305-x.
47 Yasin A, Li H, Lu Z, ur Rehman S, Siddiq M and Yang H, *Soft Matter* **10**:972–977 (2014). https://doi.org/10.1039/c3sm52666f.
48 Tian S, Wang Z, Wang X, Yang F, Shi H, Wen H *et al*., *J Appl Polym Sci* **141**:e55700 (2024). https://doi.org/10.1002/app.55700.
49 Du T, Zhao Y, Cui T, Qi Y, Abudu P, Song J *et al*., *Adv Mater Technol* **10**:2401727 (2025). https://doi.org/10.1002/admt.202401727.
50 Johnson KL, *Contact Mechanics*. Cambridge University Press, Cambridge, England, pp. 1–452 (1987).
51 Hertz H, *J Reine Angew Math* **1880**:156–171 (2009). https://doi.org/10.1515/crll.1882.92.156.
52 Boon N and Schurtenberger P, *Phys Chem Chem Phys* **19**:23740–23746 (2017). https://doi.org/10.1039/C7CP02434G.
53 Samusawa I and Shiotani K, *Corros Sci* **90**:266–275 (2015). https://doi.org/10.1016/j.corsci.2014.10.020.
54 Hu X, Guo J, Wang Y et al., Spectrochimica acta. *Part A, Molecular and biomolecular spectroscopy*, **74**:48–51 (2009). https://doi.org/10.1016/j.saa.2009.04.027.
55 Zhu K, Da Yu, Chen X and Song G, *Food Hydrocolloids* **87**:260–269 (2019). https://doi.org/10.1016/j.foodhyd.2018.08.019.
56 Nonoyama T, Lee YW, Ota K, Fujioka K, Hong W and Gong JP, *Adv Mater* **32**:e1905878 (2020). https://doi.org/10.1002/adma.201905878.
57 Fei R, George JT, Park J, Means AK and Grunlan MA, *Soft Matter* **9**:2912–2919 (2013). https://doi.org/10.1039/c3sm27226e.
58 Nothdurft K, Müller DH, Mürtz SD, Meyer AA, Guerzoni LPB, Jans A *et al*., *J Phys Chem B* **125**:1503–1512 (2021). https://doi.org/10.1021/acs.jpcb.0c10430.
59 Bertrand T, Peixinho J, Mukhopadhyay S and MacMinn CW, *Phys Rev Appl* **6**:64010–64030 (2016). https://doi.org/10.1103/PhysRevApplied.6.064010.
60 Sakai T ed, *Physics of Polymer Gels*. Wiley-VCH, Weinheim (2020).
61 Pastoriza A, Pacios IE and Piérola IF, *Polym Int* **54**:1205–1211 (2005). https://doi.org/10.1002/pi.1832.
62 Kabra BG and Gehrke SH, *Polym Commun* **32**:322 (1991).

Polymer International published by John Wiley & Sons Ltd on behalf of Society of Chemical Industry.